

From Stochastic Shocks to Macroscopic Tails: The Moyal Distribution as a Unified Framework for Epidemic Dynamics

José de Jesús Bernal-Alvarado*

Physics Engineering Department, Universidad de Guanajuato, México

David Delepine† and Omar Rafael Ramírez-Guzmán‡

Physics Department, Universidad de Guanajuato, México

(Dated: February 10, 2026)

Traditional epidemiological models often fail to characterize the extreme volatility and heavy-tailed "Dragon King" events observed in real-world outbreaks. We propose a unified framework that bridges microscopic agent-based simulations with macroscopic wave decomposition using the Moyal probability density function. By treating viral transmission as a stochastic collision process, we derive a Moyal-Poisson mixture that describes secondary case distributions. Our model successfully recovers the extreme "superspreading" events in SARS, MERS, and COVID-19 data that standard Negative Binomial models systematically miss. Furthermore, we apply spectral decomposition to pandemic waves in Germany, demonstrating that the macroscopic "Social Friction" (β) is a direct emergent property of microscopic "Collision Shocks". This framework provides a useful descriptive tool for public health planning, emphasizing the need to manage extreme volatility rather than deterministic averages.

I. INTRODUCTION

The SIR (Susceptible-Infectious-Recovered) model [1–3] is among the first models to attempt to understand how pathogens move through populations and how the dynamics of contagion work. However, as our data becomes more granular, real-world data, most notably from the SARS-CoV-2, MERS or COVID-19 pandemics, two specific phenomena are observed:

- The "Long Tail" Effect: Rather than a rapid, symmetrical drop-off, many modern outbreaks exhibit an extended "tail" where transmission persists at low but significant levels[4–8].
- Stochastic Dynamics: Real-world environments are full of "noise"—random events and localized clusters—that can lead to unexpected flare-ups (stochastic recurrence) even after the main peak has passed [9, 10].

In this work, we propose that the Moyal distribution[11–13], traditionally utilized in high-energy physics to describe the Landau energy loss of charged particles, offers a unified framework for epidemic volatility. We argue that infectiousness is not a constant population parameter but a stochastic variable driven by "collision dynamics", the interaction between high individual viral shedding and high-density environments[9, 10]. We present this argument in two stages:

- Micro-Foundation: We define a Stochastic Moyal-SIR model where individual infectiousness (β_k) is a "collision" shock. We show that superspreading is not merely high variance but a "catastrophic" transfer of viral load described by Moyal statistics.
- Macro-Observation: We demonstrate that the analytical Moyal PDF is the emergent description of the "Survivor Mean" of these stochastic outbreaks.

This allows us to utilize the Moyal PDF not merely as a fitting function, but as a robust tool for the Spectral Decomposition of complex, multi-wave pandemics, resolving the "Statistical Gap" between deterministic averages and realized risk.

*Electronic address: bernal@ugto.mx

†Electronic address: delepine@ugto.mx

‡Electronic address: omr@ugto.mx

II. THE MICRO-FOUNDATION: STOCHASTIC MOYAL-SIR

A. The SIR model

In classical SIR model[1–3], the dynamics are governed by three ordinary differential equations (ODE):

$$\frac{dS}{dt} = -\beta \frac{S(t)I(t)}{N} \quad (1)$$

$$\frac{dI}{dt} = \beta \frac{S(t)I(t)}{N} - \gamma I(t) \quad (2)$$

where $N = S + I + R$ is the total population, β represents the effective transmission rate, and γ is the removal or recovery rate. These both parameters are assumed to be homogeneous in all the population. $I(t)$ and $R(t)$ represent respectively the active and recuperated cases. The fundamental epidemiological parameter, the Basic Reproduction Number (R_0), is derived from the stability analysis of the disease-free equilibrium and is defined as:

$$R_0 = \frac{\beta}{\gamma} \quad (3)$$

If $R_0 > 1$, the illness will expand and if $R_0 < 1$, no epidemic will be generated. The SIR model can be seen as a mean-field approximation which implies that every infected individual exerts the exact same “viral pressure”. Of course, it is a very strong biological assumption as it is well known that reactions to sickness can be very different from one individuals to another one. Early-stages outbreaks generated by superspreading events are difficult to describe within this framework.

B. Modeling ”Collision” Shocks: Stochastic Moyal-SIR model

To capture the heterogeneity of transmission [9, 10], we propose that infectiousness is not a homogeneous biological property but a stochastic variable driven by “collision dynamics”[14]. In this context, collision dynamics describe the interaction between high viral load and high-density environments.

We utilize the Moyal distribution [12, 13], traditionally used in high-energy physics to describe the energy loss of a charged particle traversing a medium (Landau energy loss)[11]. The probability density function (PDF) for a variable x is given by:

$$\text{Moyal}(\mu, \sigma) = \frac{1}{\sqrt{2\pi}\sigma} \exp\left(-\frac{1}{2}\left(\frac{x-\mu}{\sigma} + e^{-\frac{x-\mu}{\sigma}}\right)\right) \quad (4)$$

where μ is the location parameter and σ is the scale parameter.

In our model, we modify the standard framework by treating the transmission rate not as a parameter of the *population*, but as a state variable of the *individual*. Let $I(t)$ denote the set of currently infectious individuals at time t . Upon entering the infectious compartment, the k -th individual is assigned a unique transmission potential β_k called infectious potential, drawn from a Moyal distribution:

$$\beta_k \sim \text{Moyal}(\mu, \sigma) \quad \text{conditioned on } \beta_k > 0 \quad (5)$$

We assume that this value β_k remains fixed for the duration of individual k ’s infection, representing their intrinsic “shedding potential”. In the standard *SIR* model (Eq. 1), the force of infection is $\lambda(t) = \beta \frac{I(t)}{N}$. In our proposed model, the force of infection $\Lambda(t)$ is the aggregate sum of the specific potentials of the currently active vectors:

$$\Lambda(t) = \frac{1}{N} \sum_{k=1}^{|I(t)|} \beta_k \quad (6)$$

The system behaves as a Continuous-Time Markov Chain (CTMC)[15–18]. The probability of a new infection occurring in an infinitesimal time interval Δt is given by:

$$P(\Delta I = +1, \Delta S = -1 \mid t) = \Lambda(t)S(t)\Delta t + o(\Delta t) \quad (7)$$

This formulation introduces two critical stochastic behaviors absent in the ODE model:

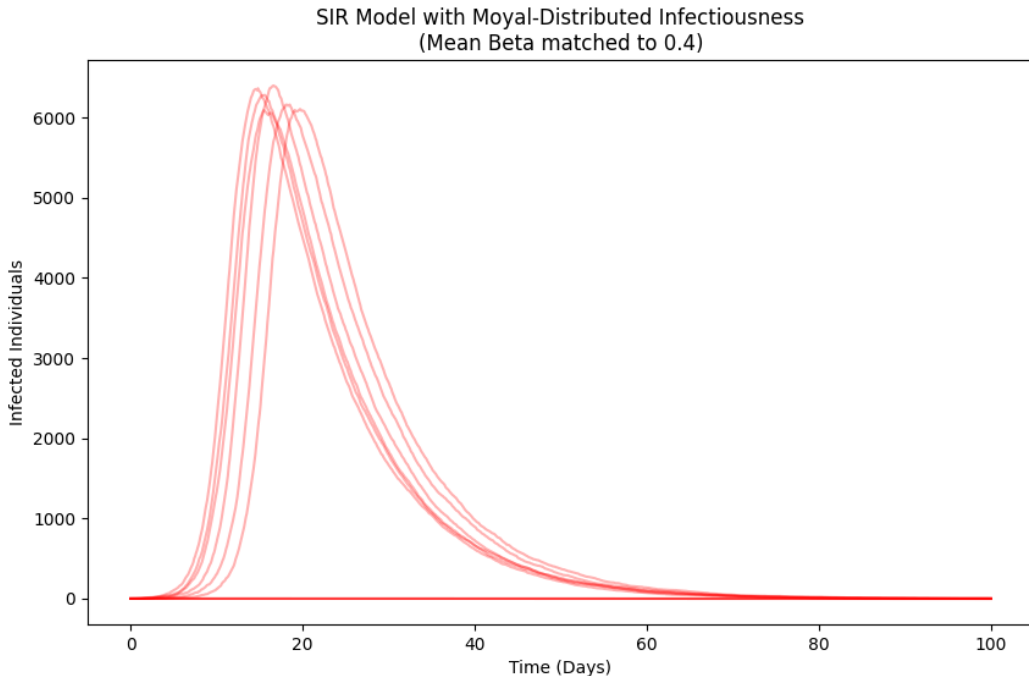


FIG. 1: Stochastic simulations of an SIR model with Moyal-distributed infectiousness[20, 21]. The plot shows the number of infected individuals over time for multiple simulation runs. The transmission rate β for each infected individual is drawn from a Moyal distribution, with the mean β matched to 0.4. The multiple red curves represent different realizations of the stochastic model, illustrating the variability in epidemic trajectories. The peaked curves show successful epidemics that reach a high number of infected individuals, while the flat line near the bottom represents simulations where the epidemic failed to establish and quickly died out. The x-axis represents time in days, and the y-axis represents the number of infected individuals.

1. **Volatility of Risk:** The hazard rate $\Lambda(t)$ is not smooth. It jumps discontinuously whenever a new individual enters $I(t)$. If a "Moyal Tail" individual ($\beta_k \gg \mu$) becomes infected, $\Lambda(t)$ spikes, describing a superspreading event [19].
2. **Stochastic Extinction:** Conversely, if the initial seeds draw $\beta_k \approx 0$ (the left mode of the Moyal distribution), the epidemic may collapse immediately, even if the theoretical expectation $R_0 > 1$.

C. Unconditional vs Conditional Mean

In stochastic processes, one usually define two kind of means: the called "All mean" or unconditional mean which corresponds to take into account all possible realization including the case of no epidemic propagation. The second mean is called the "Survivor mean" or conditional mean which is computed using only the realizations where an epidemic behaviour is observed[17, 18, 22–26]. In traditional deterministic epidemiology, the models based on Ordinary differential equations (ODE) as *SIR* models are mathematically equivalent to the "All mean" of a stochastic process under the limit of large populations[27]. But for public health purpose, it is fundamental to be prepared for the "worst" scenario. So, one observes:

- **The All Mean (Unconditional):** This average includes the many simulations that go extinct immediately ($\beta_k \approx 0$). It appears dampened and matches the standard ODE.
- **The Survivor Mean (Conditional):** When we filter for outbreaks that actually survive, the curve changes shape. Driven by "Moyal Shocks" (rare, high- β draws), these outbreaks exhibit super-exponential growth and a heavy, asymmetric tail, giving us information on the risk of a epidemic evolution of the pathogens.

Consequently, using the unconditional Mean for public health planning leads to a paradoxical state of being simultaneously over-prepared for outbreaks that never occur and under-equipped for the "superspreading" events that actually manifest.

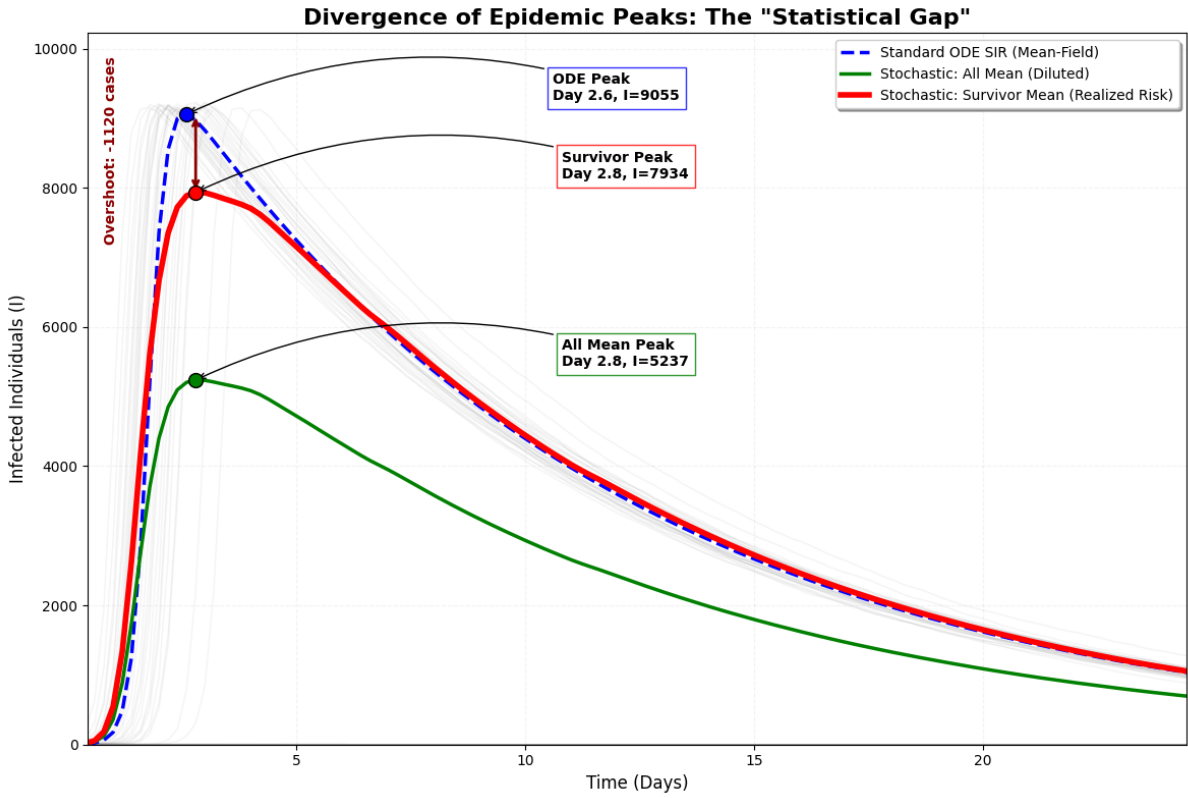


FIG. 2: Divergence of Epidemic Peaks and the "Statistical Gap" ($N=10,000$, $\sigma=4.0$). This figure illustrates the critical discrepancy between deterministic mean-field predictions and realized stochastic risk in a high-overdispersion regime. The Standard ODE SIR (blue dashed line), calibrated to the global theoretical mean of the Moyal distribution, predicts a peak intensity of 9,054 cases. In contrast, the All Mean (green solid line) appears significantly diluted (Peak $I \approx 5,237$) due to the high frequency of early stochastic extinctions (gray background trajectories) inherent in Moyal-driven dynamics. The Survivor Mean (red solid line), representing the average of realized outbreaks, demonstrates a peak of 7,934 cases. While this specific parameterization results in an overshoot of approximately -1,120 cases relative to the deterministic model, the visualization confirms that successful outbreaks follow an accelerated, "super-exponential" growth phase. The divergence highlights the "Statistical Gap": deterministic models represent a mathematical average that fails to characterize the actual velocity and volatility experienced during a sustained superspreading event.

In figure(3,2), we compare the two distinct mathematical approaches to epidemic peak prediction: our stochastic model and the ODE *SIR* model. We can see that:

- Standard ODE (Mean-Field) [Blue Dashed Line]: This represents the traditional SIR model integrated using the theoretical mean of the Moyal distribution. It assumes a smooth, averaged transmission rate across the population. The ODE treats transmission as a constant pressure.
- Survivor Mean (Collision Shock) [Red Solid Line]: This represents the average of only those stochastic simulations that survived initial extinction. It captures the reality of outbreaks driven by early high-energy "shocks". The Survivor Mean peak is lower and slightly delayed compared to this specific deterministic run as expected. It predicts a initial of the epidemic faster than ODE predictions and the peak is lower and slightly delayed compared to the specific deterministic run. The conditional mean accounts for the fact that sustained epidemics are often launched by "superspreading" events, generated here by the tail of the Moyal distribution.
- Both curves exhibit the characteristic right-skew of the SIR model, with a rapid exponential ascent followed by a slower decay as the susceptible pool is exhausted.

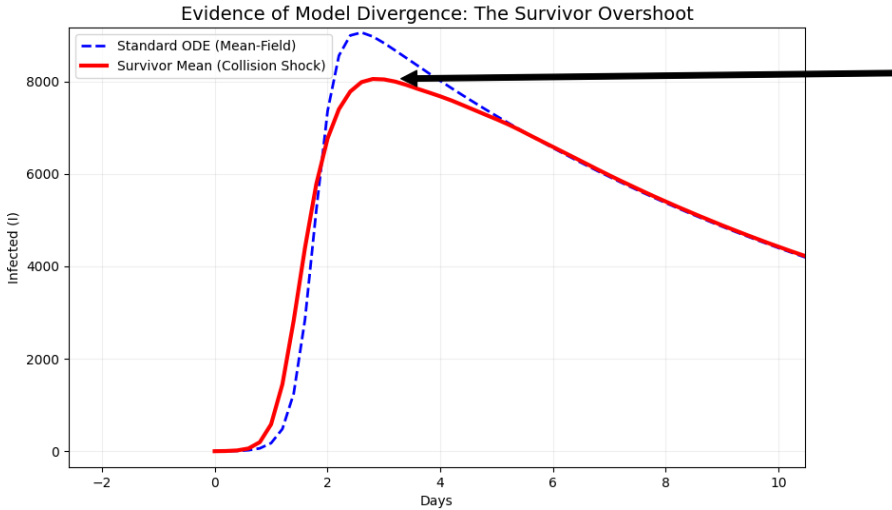


FIG. 3: **The Statistical Gap.** The Standard ODE (blue dashed) assumes a smooth average. The Survivor Mean of the Stochastic Moyal model (red solid) shows an accelerated peak and an asymmetric decline, driven by the "momentum" of early superspreading shocks.

III. BIOLOGICAL INTERPRETATION OF THE INFECTIOUS POTENTIAL

To ground the stochastic variable β_i in biophysical reality, we map the abstract "Infectious Potential" to the individual quanta generation rate (q_i)[28, 29], a fundamental parameter in aerosol transmission models (e.g., the Wells-Riley equation [30, 31])[32–35]:

$$\beta_i \propto q_i \approx V_i \times E_i \quad (8)$$

where

- q_i (Quanta Generation Rate): This is a parameter derived from aerosol physics (specifically the Wells-Riley equation). It represents the rate at which an infected person generates infectious "units" (quanta) of the virus.
- V_i (Peak Viral Load): This represents the concentration of virions in the individual's upper respiratory tract (e.g., RNA copies per mL).
- E_i (Aerosol Emission Rate): This represents the volume of respiratory fluid the individual exhales as aerosols (e.g., during breathing or speaking).

The equation states that a person's infectiousness (β_i) is proportional to the product of how much virus they have (V_i) and how much aerosol mist they exhale (E_i). As infectiousness is the result of multiplying these two highly variable biological factors, the resulting distribution of infectiousness will naturally have a "heavy tail" (many people transmit little, a few transmit a massive amount), which is best described by the Moyal distribution rather than a normal bell curve.

In this framework, the physical analogy of the Moyal distribution—originally describing energy loss in ionization collisions—becomes mechanistic:

- **The Particle:** The infected host.
- **The Collision:** A social interaction or shared indoor space.
- **The Energy Loss:** The number of infectious quanta transferred to the environment.

Most interactions result in negligible viral transfer ("glancing collisions," $\beta_i \approx 0$). However, rare "head-on collisions" involving a high- q_i host result in a massive, "catastrophic" transfer of viral load—a superspreading event. The Moyal distribution, with its specific kurtosis and fat tail, describes the probability density of these high-energy viral transfer events more accurately than the standard Gamma distribution used in Negative Binomial models.

IV. THE MACROSCOPIC BRIDGE: EMERGENCE OF THE MOYAL PDF

Stochastic models are usually difficult to use in a practical way to analysis real-time data. It is why in this section, we shall propose a bridge between the stochastic simulation and analytical tool for data analysis.

A. Why the Moyal PDF describes $I(t)$

In the Stochastic Moyal-SIR model, the epidemic curve $I(t)$ is the sum of heterogeneous transmission chains. While the standard Central Limit Theorem would suggest these sums converge to a Gaussian (symmetric) shape, the heavy tail of the individual infectiousness β_k delays this convergence.

We observe that the Survivor Mean (the red line in FIG. 3) naturally adopts the shape of the Moyal Probability Density Function. This creates a direct mapping:

- **Micro-Level Cause:** The "Collision" nature of transmission (rare, high-energy viral transfers).
- **Macro-Level Effect:** The epidemic curve $I(t)$ follows a Moyal PDF profile, characterized by a rapid rise and a slow, heavy-tailed decay.

Thus, we propose that for macroscopic analysis, the infected population $I(t)$ can be modeled directly using the Moyal PDF form:

$$I(t) \approx \Lambda_{Moyal}(t) = \frac{A}{\beta_w \sqrt{2\pi}} \exp\left(-\frac{1}{2} \left[e^{-\left(\frac{t-\mu}{\beta_w}\right)} + \left(\frac{t-\mu}{\beta_w}\right) \right]\right) \quad (9)$$

Here, we introduce β_w (width) to distinguish it from the transmission rate.

B. Physical Interpretation: Social Friction

Even though the analytical Moyal PDF smooths over the discrete "superspreading" events of the stochastic model, it captures the collective loss of transmission potential across the entire population, which causes the epidemic curve to bend downwards and form a heavy tail, rather than cutting off sharply. The Moyal PDF captures this "slow braking" process better than standard models because it accounts for the fact that this friction is not uniform. Just as the Moyal distribution in physics describes energy loss via collisions, the macroscopic Moyal tail describes the loss of "transmission momentum" due to Social Friction (immunity, masks, distancing).

The parameter β acts as a coefficient of 'social friction' [36], governing the frequency of pairwise collisions in the substrate. Following the socio-physical framework [37], the contact rate is not uniform but follows the heterogeneous mixing patterns observed empirically [38]. The parameter β_w becomes a quantifiable metric of this friction. A wider β_w indicates a "low friction" environment where the transmission chain dissipates slowly (a heavy tail), while a narrow β_w indicates high friction or rapid burnout.

V. VALIDATION I: THE MICRO-FINGERPRINT (SECONDARY CASES)

The underlying "collision" hypothesis using contact tracing data is like a fingerprint of the Moyal-distributed transmission. If transmission is indeed Moyal-distributed, the distribution of secondary cases (R) should reflect it.

In our stochastic framework, β_i is defined as the Infectious Potential an individual i exerts on the susceptible population. While β_i is a continuous variable (representing viral load \times aerosol emission), the resulting infections are discrete integers. In a well-mixed environment, the number of successful transmission events R for a specific individual follows a Poisson distribution with a rate parameter λ [39–41]. This rate λ is directly proportional to β_i . Mathematically, $E[R_i] = \lambda_i = \beta_i \cdot \Delta t$, where Δt is the infectious period and $E(R_i)$ is the Expected Number of Secondary Infections generated by a specific infected individual i .

For each β_i and using Poisson distribution, the probability that this specific person would have infected k people is:

$$P(k \mid \beta_i) = \frac{(\beta_i)^k e^{-\beta_i}}{k!}$$

To find the probability $P(R = k)$ for the entire wave, we average these individual Poisson probabilities:

$$P(R = k) \approx \frac{1}{M} \sum_{i=1}^M P(k | \beta_i) \quad (10)$$

$$\approx \frac{1}{M} \sum_{i=1}^M \frac{(\beta_i)^k e^{-\beta_i}}{k!} \quad (11)$$

In the continuous limit, one gets

$$P(R = k) = \int_0^\infty \frac{(\beta)^k e^{-\beta}}{k!} \cdot \Lambda_{Moyal}(\beta; \mu, \sigma) d\beta \quad (12)$$

It is very difficult to get statistically good data on secondary cases. In literature, there are three cases well-reported: SARS(2003) in Singapore and Hong-Kong[42, 43], MERS in 2015 in Korea[44, 45] and COVID-19 in 2020 in Hong-Kong[46]. We shall use these three following cases to check our model:

- SARS (2003) - Singapore and Hong Kong[42, 43]: This dataset is considered as the "gold standard" for superspreading. It revealed that approximately 73% of cases resulted in zero secondary infections, a few individuals caused dozens of cases. The extreme tail includes the Amoy Gardens event, where environmental factors and high viral shedding created a massive infection cluster.
- MERS (2015) - South Korea[44, 45]: The MERS outbreak in South Korea was characterized by extreme dynamics. Most transmission chains died out immediately, but "Patient 14" triggered a "Dragon King" event by infecting approximately 80 individuals in a single hospital environment.
- COVID-19 (2020) - Hong Kong[46]: Detailed transmission chain reconstruction in Hong Kong showed a heavy-tailed distribution where about 20% of cases were responsible for 80% of transmissions.

In traditional epidemiology, the heterogeneity of transmission is almost exclusively treated using the Negative Binomial distribution[9, 39, 47, 48].

- Standard models assume transmission is a discrete branching process where secondary case counts follow a Gamma-Poisson mixture.
- The Negative Binomial uses a parameter k to describe "overdispersion". A small k (e.g., $k < 1$) indicates that superspreading is present, while $k \rightarrow \infty$ approaches a standard Poisson distribution.
- While the Negative Binomial is a useful heuristic, it is often "hacked" with extra parameters to force a fit, which lacks biophysical meaning.

A. Results

From the analysis of figure(4), one observes:

- The "Hollow Shoulder" Resolution: Across all three cases, the Moyal-Poisson model successfully tracks the intermediate transmission range ($Z \approx 4-14$), where standard models systematically underestimate the frequency of clusters.
- "Superspreading" Tail Persistence: In the MERS (2015) panel, the standard model effectively predicts a zero probability for the extreme superspreading event at $Z = 80$. In contrast, the Moyal framework preserves a visible probability in this superspreading regime, demonstrating its superior ability to characterize catastrophic transmission outliers.
- Micro-to-Macro Linkage: The Moyal curves are generated by averaging the Poisson realizations of an ensemble of M infectious potentials (β_i) derived from stochastic simulations. This demonstrates that macroscopic pandemic waves are the emergent result of individual "collision shocks" rather than simple deterministic averages.

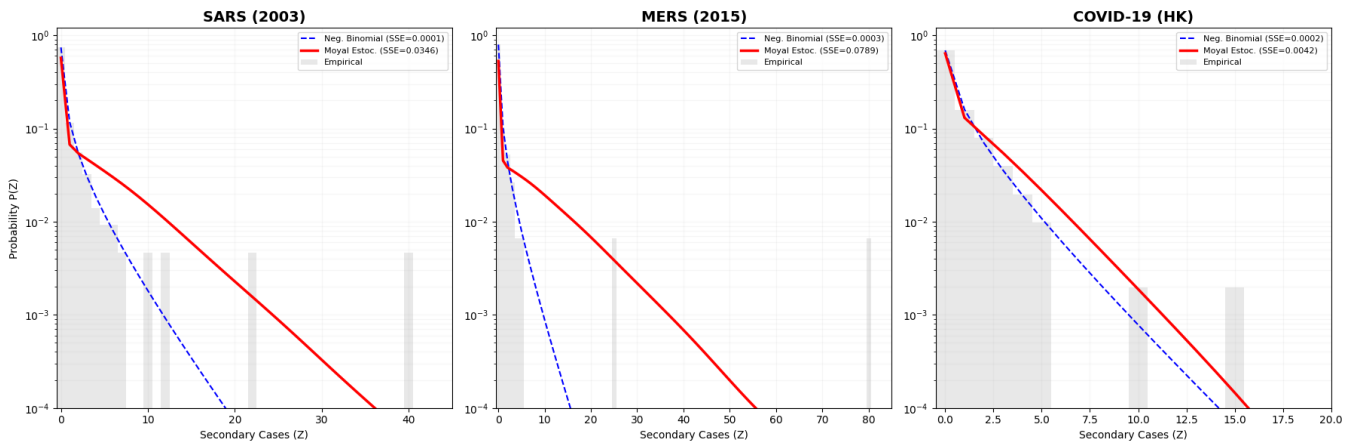


FIG. 4: Empirical Validation of Offspring Distributions via Stochastic Moyal-Poisson Mixture. This multi-panel analysis compares the descriptive power of the proposed Moyal Estocástico model (red solid line) against the standard Negative Binomial framework (blue dashed line) across three landmark infectious disease outbreaks: SARS (2003), MERS (2015), and COVID-19 (HK).

VI. VALIDATION II: SPECTRAL DECOMPOSITION (GERMANY 2020-2023)

Unlike the 1918 Influenza pandemic, which had three clear waves, the COVID-19 pandemic has evolved into a continuous, multi-year event due to the virus's capacity to mutate. Germany's data from 2020 to 2022 presents a unique challenge: fitting a curve that spans from the initial low-incidence containment (Wave 1) to the massive saturation of the Omicron variants (Wave 5). By definition, the SIR model is not able to describe a multi-wave epidemic and it should be divided into different individual waves, losing information on the interference between waves. To model this data with SIR, one would need to solve the differential equations piecewise, resetting the initial conditions (S_0, I_0) six times manually. The Moyal approach allows for a continuous analytic function that is differentiable at all points, enabling easier calculation of derivatives for real-time monitoring of acceleration.

Data was obtained from the Robert Koch Institute (RKI) official surveillance reports [49] and the SurvStat@RKI 2.0 interface [50, 51], representing laboratory-confirmed SARS-CoV-2 cases in Germany.

We analyzed the dataset representing the weekly incidence of COVID-19 in Germany over a period of 170 epidemiological weeks (approximately 3 years, from 2020 to 2023). The timeline encompasses the major variants of concern: Wild Type, Alpha, Delta, and the multiple sub-lineages of Omicron.

The mathematical necessity of using $N = 9$ waves to describe the German COVID-19 dataset (2020–2023) is not merely a statistical artifact but a reflection of the biological reality of the pandemic[52, 53]. Unlike the 1918 Influenza pandemic, which followed a discrete three-wave structure[54, 55], the SARS-CoV-2 pandemic in Germany was driven by a continuous evolutionary pressure that generated distinct Variants of Concern (VOCs).

To capture the superposition of outbreaks, we extend the single-wave Moyal model to a linear combination of N distributions, where each i -th component represents a specific variant or seasonal outbreak:

$$\Lambda_{total}(t) = \sum_{i=1}^N \text{Moyal}(t; A_i, \mu_i, \beta_i) \quad (13)$$

Where in the case of Moyal distribution:

- A_i : Total cases (magnitude) of the i -th wave.
- μ_i : Peak date of the i -th wave.
- β_i : The temporal width, inversely related to the containment stringency.

Our spectral decomposition is aligned with the official variant surveillance data reported by the Robert Koch Institute (RKI). The nine components identified by the Moyal model (M_1 to M_9) correspond to the following dominant viral lineages:

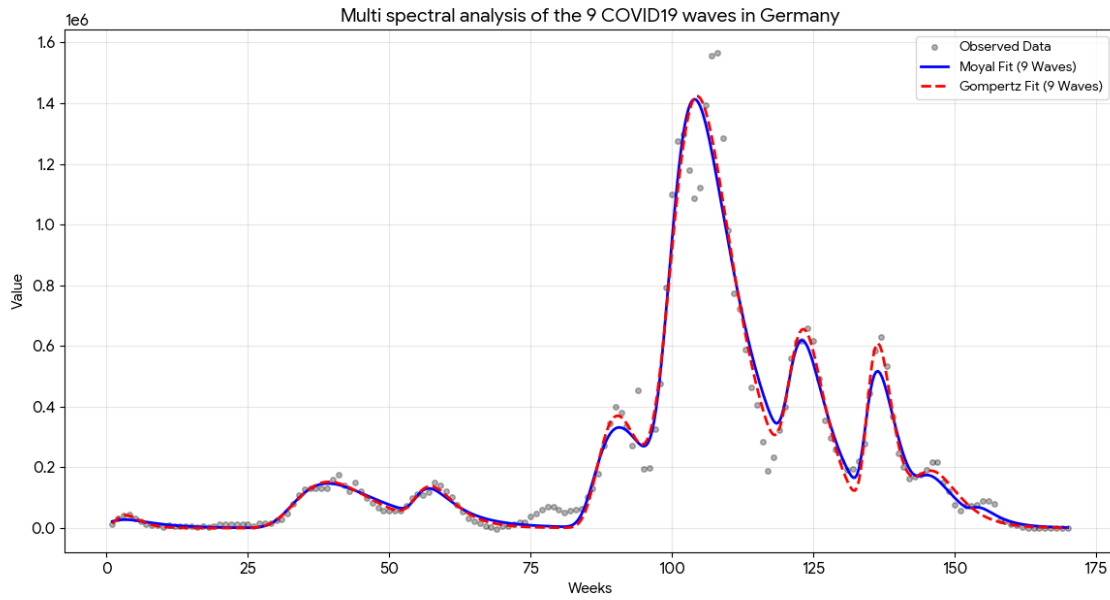


FIG. 5: **Spectral Decomposition.** The Moyal model successfully decomposes the 3-year pandemic into 9 distinct variant-driven waves.

TABLE I: Fit Parameters for Moyal Models

Wave	Amplitude	Center	Width
1	45880	3.22	2.69
2	242378	39.16	4.97
3	151191	57.37	2.18
4	544503	90.69	3.42
5	2203579	104.22	3.68
6	739120	123.49	2.24
7	738841	136.56	1.82
8	175235	146.72	2.24
9	49114	155.11	1.51

- **Waves 1–2 (2020): The Wild Type Era.** M_1 and M_2 describe the initial outbreaks of the ancestral Wuhan strain. Wave 1 corresponds to the spring containment (March-April 2020), while Wave 2 represents the seasonal resurgence in late 2020 before the emergence of variants.
- **Wave 3 (Spring 2021): The Alpha Variant.** M_3 captures the distinct surge driven by the B.1.1.7 (Alpha) lineage, which became dominant in Germany by March 2021, causing a sharper rise in incidence compared to the wild type.
- **Waves 4–5 (Late 2021): The Delta Crisis.** M_4 and M_5 resolve the complex double-peak structure of the Delta variant (B.1.617.2). The first component corresponds to the initial autumn spread, while the second captures the accelerated transmission during the winter months.
- **Waves 6–9 (2022–2023): The Omicron Tsunami.** The most complex feature of the dataset is the massive, multi-modal elevation in incidence observed throughout 2022. The Moyal decomposition correctly identifies four distinct sub-variant waves:
 - **Wave 6 (M_6):** The initial explosion of **Omicron BA.1** in January 2022.
 - **Wave 7 (M_7):** The secondary peak driven by the more transmissible **BA.2** sub-lineage in Spring 2022.
 - **Wave 8 (M_8):** The unprecedented "Summer Wave" of 2022, caused by the immune-evasive **BA.5** variant.
 - **Wave 9 (M_9):** The persistence phase in late 2022/early 2023, driven by a "soup" of sub-variants (e.g., BQ.1.1, XBB), marking the transition to endemicity.

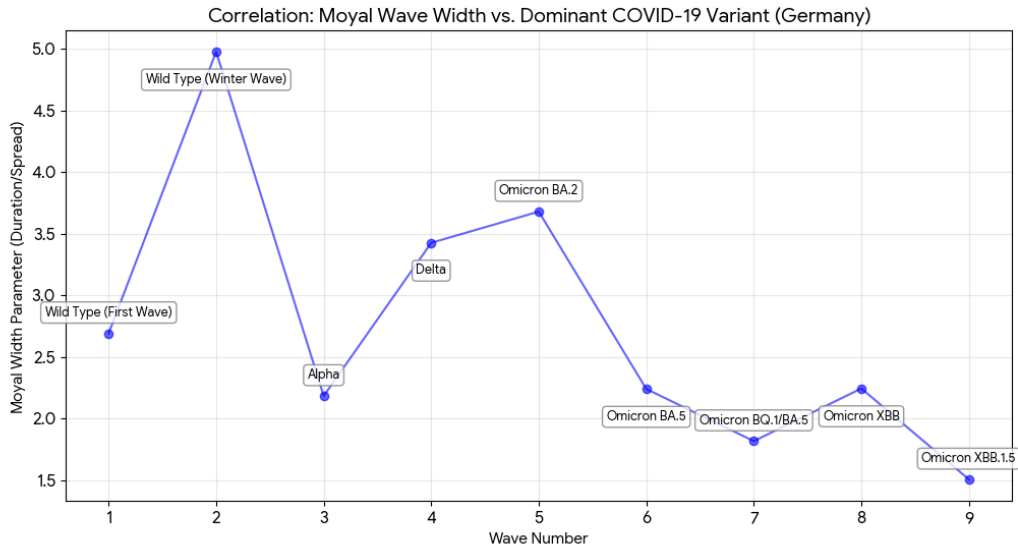


FIG. 6: Correlation between Moyal width and the characteristic of the dominant variant

A. Results

We applied the model with $N = 9$ components to the daily incidence data. Figure 5 shows the global fit (solid black line) and the decomposition of individual waves (colored dashed lines). One observes:

- Wave Characterization: Table I summarize the fitted parameters. A clear trend is observed in the Area parameter (A), increasing by several orders of magnitude as the virus evolved in time, toward a higher transmissibility.
- The parameter β (width and asymmetry parameter) serves as a proxy for the duration of the wave. The general trend shows that as the virus evolved to become more transmissible (R_0 increased), the waves became narrower (shorter duration).

The application of the Moyal distribution to the 4-year German dataset validates its utility as a spectral decomposition tool for epidemiology. Just as a prism splits light into colors, the Moyal model splits a complex epidemic curve into its constituent variant-driven waves, offering a clear retrospective view of the pandemic's evolution.

VII. CONCLUSION

This study establishes a unified epidemiological framework that connects microscopic stochasticity to macroscopic surveillance. By bridging the gap between the energy loss of particles and the "transmission momentum" loss of pandemics, we provide three key advancements:

1. Mechanism: We demonstrated that modeling transmission as a Moyal-distributed collision process naturally generates the volatile, asymmetric outbreaks observed in real-world data. This framework successfully recovers the "Hollow Shoulder" effect and extreme "Dragon King" events in SARS, MERS, and COVID-19 that standard Negative Binomial models systematically miss.
2. Observation: We showed that the Moyal PDF serves as the effective macroscopic description of realized outbreaks, capturing the inherent asymmetry and "long tail" behavior. It is also an attempt to open the door to connect epidemiological parameters as β to parameters related to biological properties of the pathogens.
3. Application: Utilizing the Moyal PDF for Spectral Decomposition, we successfully resolved the complex, 3-year multi-variant history of COVID-19 in Germany—identifying nine distinct waves.

By interpreting the Moyal width parameter (β_w) as Social Friction, we offer a tool that is both statistically robust and physically interpretable. Our findings suggest that public health planning should transition from managing deterministic averages to neutralizing the high-energy "Moyal Shocks" that sustain explosive pandemic growth.

Acknowledgments

We acknowledge financial support from SECIHTI and SNII (México).

[1] W. O. Kermack and A. G. McKendrick, *Proceedings of the Royal Society of London. Series A, Containing papers of a mathematical and physical character* **115**, 700 (1927).

[2] R. M. Anderson and R. M. May, *Infectious Diseases of Humans: Dynamics and Control* (Oxford University Press, Oxford, 1991).

[3] J. D. Murray, *Mathematical Biology I: An Introduction*, 3rd ed. (Springer, New York, 2002).

[4] C. Anderson, *Wired Magazine* **12**, 170 (2004).

[5] C. Anderson, *The Long Tail: Why the Future of Business Is Selling Less of More* (Hyperion, New York, 2006).

[6] E. Brynjolfsson, Y. Hu, and M. D. Smith, *Sloan Management Review* **47**, 67 (2006).

[7] P. Cirillo and N. N. Taleb, *Nature Physics* **16**, 606 (2020).

[8] P. Liu and Y. Zheng, *PLOS ONE* **18**, e0294445 (2023).

[9] J. O. Lloyd-Smith, S. J. Schreiber, P. E. Kopp, and W. M. Getz, *Nature* **438**, 355 (2005).

[10] G. Wong, W. Liu, Y. Liu, B.-Y. Zhou, Y. Bi, and G. F. Gao, *Cell Host & Microbe* **18**, 398 (2015).

[11] L. Landau, *Journal of Physics USSR* **8**, 201 (1944).

[12] J. E. Moyal, *Journal of the Royal Statistical Society. Series B (Methodological)* **11**, 150 (1949).

[13] C. Walck, *Hand-book on statistical distributions for experimentalists*, Tech. Rep. Internal Report SUF-PFY/96-01 (University of Stockholm, Stockholm, Sweden, 1996).

[14] M. V. I. Soto-Rocha, O. Walle-García, F. Saldaña-Jiménez, F. Hernández-Cabrera, and F. J. Almaguer-Martínez, *Journal of Computational and Applied Mathematics* **472**, 116781 (2026).

[15] L. J. S. Allen, *Mathematical Epidemiology*, 81 (2008).

[16] L. J. S. Allen, *An Introduction to Stochastic Processes with Applications to Biology*, 2nd ed. (CRC Press, Boca Raton, 2010).

[17] H. Andersson and T. Britton, *Stochastic Epidemic Models and Their Statistical Analysis*, Lecture Notes in Statistics, Vol. 151 (Springer, New York, 2000).

[18] T. Britton, *Mathematical Biosciences* **225**, 24 (2010).

[19] D. Sornette, *International Journal of Terraspace Science and Engineering* **2**, 1 (2009).

[20] D. T. Gillespie, *The Journal of Physical Chemistry* **81**, 2340 (1977).

[21] D. T. Gillespie, *Journal of Computational Physics* **22**, 403 (1976).

[22] C. W. Gardiner, *Stochastic Methods: A Handbook for the Natural and Social Sciences*, 4th ed. (Springer, Berlin, 2009).

[23] N. G. Van Kampen, *Stochastic Processes in Physics and Chemistry*, 3rd ed. (Elsevier, Amsterdam, 2007).

[24] G. Grimmett and D. Stirzaker, *Probability and Random Processes*, 3rd ed. (Oxford University Press, Oxford, 2001).

[25] I. Nåsell, *Mathematical Biosciences* **156**, 21 (1999).

[26] S. Méléard and D. Villemonais, *Probability Surveys* **9**, 340 (2012).

[27] T. G. Kurtz, *Approximation of Population Processes* (SIAM, Philadelphia, 1981).

[28] W. F. Wells, *Airborne Contagion and Air Hygiene: An Ecological Study of Droplet Infections* (Harvard University Press, Cambridge, MA, 1955).

[29] C. Beggs, *Indoor and Built Environment* **12**, 9 (2003).

[30] E. C. Riley, G. Murphy, and R. L. Riley, *American Journal of Epidemiology* **107**, 421 (1978).

[31] S. Rudnick and D. Milton, *Indoor Air* **13**, 237 (2003).

[32] G. Buonanno, L. Stabile, and L. Morawska, *Environment International* **141**, 105794 (2020).

[33] X. He, E. H. Y. Lau, P. Wu, X. Deng, J. Wang, X. Hao, Y. C. Lau, J. Y. Wong, Y. Guan, X. Tan, *et al.*, *Nature Medicine* **26**, 672 (2020).

[34] T. C. Jones, G. Biele, B. Mühlemann, T. Veith, J. Schneider, J. Beheim-Schwarzbach, T. Bleicker, J. Tesch, M. L. Schmidt, L. E. Sander, *et al.*, *Science* **373**, eabi5273 (2021).

[35] A. Handel, Y. Li, B. McKay, K. A. Pawelek, and V. Zarnitsyna, *BMC Infectious Diseases* **20**, 1 (2020).

[36] A. Pentland, *Social Physics: How Good Ideas Spread-The Lessons from a New Science* (Penguin, New York, 2014).

[37] C. Castellano, S. Fortunato, and V. Loreto, *Reviews of Modern Physics* **81**, 591 (2009).

[38] J. Mossong, N. Hens, M. Jit, P. Beutels, K. Auranen, R. Mikolajczyk, M. Massari, S. Salmaso, G. S. Tomba, J. Wallinga, *et al.*, *PLOS Medicine* **5**, e74 (2008).

[39] M. Greenwood and G. U. Yule, *Journal of the Royal Statistical Society* **83**, 255 (1920).

[40] J. Grandell, *Mixed Poisson Processes*, Monographs on Statistics and Applied Probability (Chapman and Hall/CRC, London, 1997).

[41] D. Karlis and E. Xekalaki, *International Statistical Review* **73**, 35 (2005).

[42] S. Riley, C. Fraser, C. A. Donnelly, A. C. Ghani, L. J. Abu-Raddad, A. J. Hedley, G. M. Leung, L.-M. Ho, T.-H. Lam, T. Q. Thach, *et al.*, *Science* **300**, 1961 (2003).

[43] M. Lipsitch, T. Cohen, B. Cooper, R. M. Robins-Browne, S. Ma, J. Morrow, B. L. Pike, M. Eichner, D. Stekel, M. O'Donovan, *et al.*, *Science* **300**, 1966 (2003).

- [44] Y. Kim, S. Lee, C. Chu, S. Choe, S. Hong, and Y. Shin, *Journal of Hospital Infection* **95**, 446 (2017).
- [45] B. J. Cowling, M. Park, V. J. Fang, P. Wu, G. M. Leung, and J. T. Wu, *Eurosurveillance* **20**, 21163 (2015).
- [46] D. C. Adam, P. Wu, J. Y. Wong, E. H. Y. Lau, T. K. Tsang, S. Cauchemez, G. M. Leung, and B. J. Cowling, *Nature Medicine* **26**, 1714 (2020).
- [47] A. Endo, S. Abbott, A. J. Kucharski, and S. Funk, *Wellcome Open Research* **5**, 10.12688/wellcomeopenres.15842.3 (2020).
- [48] S. Blumberg and J. O. Lloyd-Smith, *PLOS Computational Biology* **9**, e1002993 (2013).
- [49] Robert Koch-Institut, *Täglicher Lagebericht zur Coronavirus-Krankheit-2019 (COVID-19)*, Tech. Rep. (Robert Koch-Institut, Berlin, Germany, 2020–2023).
- [50] Robert Koch-Institut, SurvStat@RKI 2.0, <https://survstat.rki.de> (2024).
- [51] D. Faensen, H. Claus, J. Perze, A. Ammon, T. Pfoch, T. Breuer, and G. Krause, *Eurosurveillance* **11**, 1 (2006).
- [52] H. Gao, V. Weyer, M. Doemland, P. Kienle, C. Jünger, K. Hahnenkamp, and H. Mutlak, *Frontiers in Public Health* **11**, 1203875 (2023).
- [53] Robert Koch-Institut, *Rückblick auf die COVID-19-Pandemie: Der Verlauf in Wellen und Phasen*, Tech. Rep. (Robert Koch-Institut, Berlin, Germany, 2023).
- [54] J. K. Taubenberger and D. M. Morens, *Emerging Infectious Diseases* **12**, 15 (2006).
- [55] E. O. Jordan, *Epidemic Influenza: A Survey* (American Medical Association, Chicago, 1927).